Supporting Information
for
"Three-Dimensional Localization of an Individual Fluorescent Molecule with Angstrom Precision"

Taku Furubayashi, Kazuya Motohashi, Keisuke Wakao, Tsuyoshi Matsuda, Isao Kii, Takamitsu Hosoya, Nobuhiro Hayashi, Mahito Sadaie, Fuyuki Ishikawa, Michio Matsushita, and Satoru Fujiyoshi

Supporting Methods

Cryo-reflecting microscope.

Figure S5 shows the details of the cryo-reflecting microscope. The microscope was composed of four optical units. Reflecting optics was used in the units to avoid chromatic aberration. Excepting those in the confocal unit, the all optics in the unites were placed in an airtight stainless-steel box for mechanical stabilization (Fig. S1c). The four units were placed in a black aluminum box that was light-shielding and airtight.

Light source. The light source was a continuous-wave diode laser with wavelengths of 637 nm (OBIS637-140mW, Coherent), 660 nm (OBIS660-100mW, Coherent), 561 nm (OBIS561-50mW, Coherent) and 375 nm (OBIS375-50mW, Coherent). The laser lights were coupled with polarization-maintaining single-mode fibers, and the outputs were collimated by the objective lenses. The collimated laser light was spectrally filtered with a bandpass filter (Filter1; FF01-637/7, Semrock, for λ_{ex} = 637 nm; #65-089, Edmund, for λ_{ex} = 660 nm; FF01-561/14, Semrock, for λ_{ex} = 561 nm; FF01-377/50, Semrock, for λ_{ex} = 375 nm).

Spatial-filter unit. The first unit was a spatial-filter unit to minimize the wave front error of a light source. The laser light was focused with the plano-convex fused-silica lens Lens1 (f = 150 mm; SLSQ-25-150P, Sigma Koki) at the center of a 20-μm pinhole (PA-20, Sigma Koki). The light was diffracted through the pinhole and collimated with the silver-coated concave mirror CM1 (f_{CM1} = 250 mm; 10DC500ER.2,

Newport). The central disk of the light was identified with an iris and propagated to the second unit.

Beam-path adjustment unit and superfluid-helium cryostat. Approximately 30% of the light was reflected by the beam-splitter BS2 (PSM25-25.4C03-10-550, Sigma Koki) and was conducted to the inside of a superfluid-helium cryostat by the second unit, a beam-path adjustment unit. The two silver-coated mirrors (M3, M4) in the second unit matched the principal ray of the laser light to the optical axis of the cryo-reflecting objective. The tilt angles of the two mirrors were finely controlled by piezo-driven linear actuators (8301NF, Newport). The field of view of the reflecting objective is approximately 1 μm × 1 μm because of coma and spherical aberration.[1] The angle between the principal ray and the optical axis was adjusted within 3×10^{-4} radians. The laser light was focused on the sample by the cryo-reflecting objective[1] (f_{obj} = 2.04 mm, NA = 0.99 in superfluid helium). The sample position was moved finely with a piezo-driven cryo-scanner in the *xyz* directions (the scanning range of 30 × 15 × 30 μm^3 in the $x \times y \times z$ directions; ANSxyz100std, Attocube Systems) and coarsely with two cryo-positioners in the *xz*-directions (distance of travel = 5 mm; ANPx101, Attocube Systems). The *xyz*-positions of the stage (x_{stage}, y_{stage}, z_{stage}) were monitored with three capacitive cryo-sensors that were custom-made for cryogenic experiments (the detection range was 100–150 μm; Unipulse). The reflecting objective and three cryo-sensors were fixed with a single-component titanium holder (Fig. S1a). Components near the sample (sample holder, cryo-stages and cryo-position sensors) were chiefly composed of titanium (Figs. S1a and S1b) so that the mechanical drift due to thermal expansion was minimized. In addition to this passive stabilization, the temperature near the sample holder was controlled within 0.24 mK standard deviation using a commercial temperature controller (model 335, Lake Shore). The standard deviation was calculated from 1200 data points with the time interval and the acquisition time = 1.5 s. The *xyz*-position of the sample stage was actively stabilized using a closed-loop feedback system with three position sensors and the cryo-scanner. Consequently, the image stability of the cryo-reflecting microscope was improved to 0.05 nm standard deviation. The standard deviation was calculated from 12 data points with the time interval and the acquisition time = 64 s. The

fluorescence light from an individual fluorescent molecule was collected by the reflecting objective. Approximately 70% of the fluorescence light passed through BS2. In addition, the excitation light reflected on the sample surface was conducted with BS2 to the third unit, a beam monitor unit. The light was focused on a complementary metal oxide semiconductor sensor (ARTCAM-130MI-BW, Artray). By the image, the *z*-distance between the sample and the objective was adjusted to the focal length of the objective (f_{obj}).

Localization and confocal unit. The cryo-reflecting microscope was operated in three modes, that is, *xy*-localization (Fig. S4a), *z*-localization (Fig. 2a), and 3D confocal raster-scanning imaging (Fig. S4b). In the first operating mode for the *xyz*-localization, the fluorescence light was separated from the excitation light with two notch filters (Filter2; NF03-633E; Semrock) and propagated to the third unit, the localization unit. The fluorescence light was focused on the charge-coupled device (CCD) image sensor (DU920P-BEX2-DD, Andor) with the silver-coated concave mirror CM2 (f_{CM2} = 1000 mm, PS-SMCC-2.00-UV, CVI). The distance between CM2 and the reflecting objective was approximately $f_{CM2} + f_{obj}$ = 1002 mm to image the point spread function (PSF) correctly along the axial direction. The observed fluorescence image of a fluorescent molecule (ATTO647N) is shown in Fig. S2c. The excitation wavelength (λ_{ex}) was 637 nm. The *xy*-position of the fluorescent molecule was determined from the centroid of the central disk by a weighted-least-squares fitting of an Airy function. The weight is the reciprocal of the expected uncertainties in photons on each pixel.[2] The accumulation time for one frame was 4 s, and the readout time was 3.5 s. The total number of frames obtained was 576.

In the second operating mode for *z*-localization, a long-focal-length singlet lens (f = 5000 mm, antireflection-coated plano-convex BK7 lens; SLB-30-5000PIR1, Sigma Koki) was added before the light was propagated to the localization unit. The fluorescence light was focused in front of the CCD camera, and the spot was defocused on the imaging sensor (Fig. 2b). The defocused image was binned in 100 pixels (10 × 10 pixels) on the CCD chip (Fig. 2c). The accumulation time for one frame was 8 s and the readout time was 0.9 s. The total number of frames obtained was 576. The standard deviation of the binning image was

evaluated by a weighted-least-squares fitting of 2D Gaussian function. The weight was the reciprocal of the expected uncertainties in photons on each pixel. Because the binning image was slightly elliptical due to the polarization of the fluorescence light, the *z*-position was determined from the average of the standard deviations along the major and minor axes.

In the third operating mode for 3D confocal raster-scanning imaging, the fluorescence light propagated to the fourth unit, the confocal unit with the flat mirror M9. The fluorescence light was focused on a 300-μm pinhole (P300S, Thorlabs) with a silver-coated concave mirror CM3 (f_{CM3} = 1000 mm; PS-SMCC-2.00-UV, CVI). In the same manner as for the localization unit, the distance between CM3 and the cryo-objective was approximately $f_{CM3} + f_{obj}$ = 1002 mm. The fluorescence light was collimated with the silver-coated concave mirror CM4 (f_{CM3} = 1000 mm, PS-SMCC-2.00-UV, CVI) and separated from the excitation light with two filters (Filter3; ZET635NF, Chroma Technology, for λ_{ex} = 637 nm; NF03-658-25, Semrock, for λ_{ex} = 660 nm; ZET561NF, Chroma Technology for λ_{ex} = 561 nm; FF01-409LP, Semrock, for λ_{ex} = 375 nm). The filtered fluorescence light was coupled with a multimode fiber (core diameter = 50 μm, NA = 0.12; Fiberguide) and counted with an avalanche photodiode (SPCM-AQR16FC, Perkin Elmer). In the 3D confocal imaging, the number of fluorescence photons was plotted against the *xyz*-position of the stage. In addition, the 300-μm pinhole could be removed from the optical path. The fluorescence image in Fig. S2b was obtained without the pinhole.

Sample for the *xyz*-localization.

ATTO647N carboxylic acid, Qdot705 carboxylic acid, and Alexa Fluor 750-modified DNA were purchased from ATTO TEC, Invitrogen, and Integrated DNA Technologies, respectively. A 10^{-10} M solution of the dyes was prepared at pH = 7 in the presence of 20 mM phosphate buffer and 1.0% wt/wt polyvinyl alcohol. The solution was spin-coated on a CaF_2 substrate with the spinning speed of 3000 revolutions per minute (rpm) for the coat time of 60 s.

Optical simulation of cryo-reflecting microscope (Figs. S6 and S7).

The optical simulation of the cryo-reflecting microscope for the *z*-localization of an individual fluorescent molecule was performed using a commercial optical design software (Zemax Optic Studio 15.5). The optical layout of the simulated microscopic system is shown in Fig. S6a. A fluorescent molecule is much smaller in size than the PSF of its fluorescence; therefore, the fluorescence of the fluorescent molecule was regarded as an isotropic emission from a point source. To express the point source, the system aperture type was set to "Object Space NA = 0.96" and the apodization type was set to "Cosine Cubed, factor = 0". The polarization was linear along the *x*-axis. The wavelength was 705 nm. The detailed design of the reflecting objective has been reported.[9] A Huygens PSF was used with a pupil sampling of 128 × 128 and the image sampling of 128 × 128. The pixel size of the obtained image ("Image Delta") was 26 μm, which is the same as that of the CCD camera used.

Immunofluorescence of human cultured cells.

HeLa cells with long telomeres (LongTEL HeLa)[3] were cultured in DMEM with 10% fetal bovine serum (FBS). Immunofluorescence was performed essentially as described[4] with some modifications. Cells on optical parallels (OPB-05C02-P, OptoSigma) were pre-permeabilized for 5 min in ice-cold CSK buffer (10 mM PIPES (pH 6.8), 100 mM NaCl, 300 mM sucrose, 3 mM $MgCl_2$) containing 0.1% Triton X-100, fixed for 15 min in 4% paraformaldehyde, and permeabilized for 5 min in PBS containing 0.2% Triton X-100. DNA was counterstained with Hoechst 33342. Antibodies used were as follows: Anti-human TRF1 rabbit polyclonal (429), anti-human POT1 mouse monoclonal (43B7)[3], Alexa 660-conjugated anti-rabbit (A21074, Invitrogen), Alexa 568-conjugated anti-mouse (A11031, Invitrogen).

Supporting Discussion

Optical simulation for the *xyz*-localization of an individual fluorescent molecule.

We carried out optical simulations for the cryo-reflecting microscope for *z*-localization. The optical layout of the simplified setup used in the simulation is shown in Fig. S6a. An individual fluorescent molecule is located at the focal point of an objective. The fluorescence of the individual fluorescent molecule is collected by the reflecting objective and focused by a combination of a plano-convex lens and a concave mirror. The theoretically predicted PSF of the fluorescence of the individual fluorescent molecule on the CCD detector is shown in Fig. S6b. The bright central disk appears with concentric bright rings. The defocused PSF image depends not only on the *z*-position of the fluorescent molecule but also on the wavelength of fluorescence (λ_{fluo}). To exclude the diffraction pattern, the pixels of the PSF of 128 × 128 pixel^2 (Fig. S6b) was binned to obtain the PSF of 12 × 12 pixel^2 (Fig. S6c). The focal length of the additional lens (5000 mm) was chosen from the commercially available lenses so that the 10 × 10-binning fluorescence image (Fig. S6c) was best fitted by a 2D Gaussian function. As seen in Fig. S6c, the shape of the binning image resembles a Gaussian function (blue curves).

The standard deviation of the binning image on the *xy*-plane ($s_{\mathrm{xy;bin}}$) was evaluated using a weighted least-squares fitting of a Gaussian function. The weight is the reciprocal of the expected uncertainties in photons on each pixel. The fitting result of $s_{\mathrm{xy;bin}}$ is linearly proportional to the *z*-position of the individual fluorescent molecule from –40 nm to 40 nm against the focal point (Fig. S6d). The slope (dz / $ds_{\mathrm{xy;bin}}$) was 1.4. In practice, $s_{\mathrm{xy;bin}}$ is calculated from the average of the standard deviations along the major and minor axes; thus, the *z*-localization error (Δz) is reduced by a factor of $\sqrt{2}$,

$$\Delta z = \frac{dz}{ds_{\mathrm{xy;bin}}} \frac{\Delta s_{\mathrm{xy;bin}}}{\sqrt{2}} \cong \Delta s_{\mathrm{xy;bin}}. \quad (1)$$

The error $\Delta s_{\mathrm{xy;defocus}}$ is caused by the photon shot noise ($\delta_{\mathrm{z;photon}}$), the pixelation noise ($\delta_{\mathrm{z;pix}}$), the mechanical drift of the microscope ($\delta_{\mathrm{z;drift}}$), and the background noise ($\delta_{\mathrm{z;back}}$).[2,5] The total z-localization error can be expressed by

$$\Delta z \cong \Delta s_{\mathrm{xy;bin}} = \sqrt{{\delta_{\mathrm{z;photon}}}^2 + {\delta_{\mathrm{z;pix}}}^2 + {\delta_{\mathrm{z;drift}}}^2 + {\delta_{\mathrm{z;back}}}^2} = \sqrt{\frac{{s_{\mathrm{xy;bin}}}^2 + \frac{{a_{\mathrm{bin}}}^2}{12}}{N} + {\delta_{\mathrm{z;drift}}}^2 + {\delta_{\mathrm{z;back}}}^2} \quad (2)$$

where a_{bin} is a pixel in the binning image. In the simple case of $\delta_{\mathrm{z;drift}}$ and $\delta_{\mathrm{z;back}} = 0$, Δz is expressed by

$$\Delta z \cong A_z \frac{s_{\mathrm{xy;bin}}}{\sqrt{N}}. \quad (3)$$

The pixel size a_{bin} is the pixel size of the binned image (530 nm) and $s_{\mathrm{xy;bin}}$ was evaluated to be 560 nm from the optical simulation in Fig. S6c. The theoretical proportional coefficient $A_{\mathrm{z}}^{\mathrm{theory}}$ was 1.0.

We simulated the z-localization error (Δz) in our cryo-reflecting microscope. The photon noise was assumed to follow a Poisson distribution. A series of Poisson-noised images was simulated with $N = 10^2$, 10^3, 10^4, and 10^5 (Fig. S7a). In the simulation of Δz, 1000 noised images were generated for each number of photons. The standard deviations of the 1000 noised images ($s_{\mathrm{xy;bin}}$) were evaluated with the weighted least-squares fitting of 2D Gaussian function. From Fig. S6d, the z-position of an individual fluorescent molecule is proportional to 1/1.4 of $s_{\mathrm{xy;bin}}$. The simulated errors for Δz are shown as a function of N (green circles in Fig. S7b). The proportionality factor of the simulation ($A_{\mathrm{z}}^{\mathrm{sim.}}$) in Eq.3 was simulated as 1.3, which is 1.3 times the theoretically predicted factor ($A_{\mathrm{z}}^{\mathrm{theory}} = 1.0$). This variance might be due to the difference between the fitting function (Gaussian) and the shape of the binning image in Fig. S6c.

The xy-position of the individual fluorescent molecule was obtained from a centroid of PSF at $z = 0$ nm. The optical setup is shown in Fig. S4a. The xy-centroids were evaluated from of a bright disk in PSF using a weighted least-squares fitting of Airy function The weight is the reciprocal of the expected uncertainties in photons on each pixel). The number of fluorescence photons inside the bright disk (N_{disk}) is expressed by $N \times EE_{1\mathrm{st}}$, where $EE_{1\mathrm{st}}$ is an encircled energy inside the first dark ring. The theoretically predicted xy-localization error (Δxy) can be expressed by

$$\Delta xy = \sqrt{\frac{{s_{\mathrm{xy;disk}}}^2 + \frac{a^2}{12}}{N_{\mathrm{disk}}} + {\delta_{\mathrm{xy;drift}}}^2 + {\delta_{\mathrm{xy;back}}}^2}, \quad (4)$$

where a is the pixel size in the image (53 nm).[2]

From the optical simulation of PSF, the theoretical values are $EE_{1st} = 0.40$ and $s_{xy;disk} = 109$ nm. The simple case of $\delta_{z;drift}$ and $\delta_{z;back} = 0$ gives the equation,

$$\Delta xy \cong A_{xy} \frac{s_{\mathrm{xy:disk}}}{\sqrt{N}}. \quad (5)$$

The proportional coefficient for the *xy*-localization in theory $A_{\mathrm{xy}}^{\mathrm{theory}}$ was 1.6.

In a manner similar to the *z*-localization, the photon noise was assumed to follow a Poisson distribution. The *xy*-localization error Δ_{xy} was simulated as a function of N (pink circles in Fig. S7c). The simulated errors (pink circles) are in good agreement with the theoretical curve (black curve). The proportional coefficient for the *xy*-localization in the simulation ($A_{\mathrm{xy}}^{\mathrm{sim.}}$) was evaluated as 1.7.

Experimental results for the *xyz*-localization of an individual fluorescent molecule.

The experimental results for the cryo-localization microscopy of an individual ATTO647N molecule are summarized in Table S1. The localization errors were 0.53 nm (Δx), 0.31 nm (Δy) and 0.90 nm (Δz), which are shown in Fig. 3b. The accumulation times t were 64 s (*xy*) and 256 s (*z*). The centroids in the *xy* direction can be evaluated from the same 2D image. The total time for *xy*-localization was 64 s. The *xy*-localization errors are inversely proportional to the square root of the number of electrons detected by a CCD camera. The number of electrons is shown as N in Table S1. The standard deviations of s were evaluated from the observed images (see Figs. S2c and 2c). From the experimental values of Δr, N, and s, the experimental coefficients in Eqs. 3 and 5 were calculated as 3.8 ($A_{\mathrm{x}}^{\mathrm{Exp.}}$), 2.2 ($A_{\mathrm{y}}^{\mathrm{Exp.}}$), and 3.0 ($A_{\mathrm{z}}^{\mathrm{Exp.}}$). The experimental coefficients are approximately twofold of the simulated coefficient, which suggests that the *xyz*-localization errors are twofold greater than that in the case of δ_{drift} and $\delta_{back} = 0$. We preliminarily tested that the temperature of the driver box for the *x*-position sensors was stabilized; Δx then became similar to Δy. The

y-localization might have been due to the thermal drift of the feedback loop circuit. Finally, we consider the *z*-localization experiment. In Eq. 2, $\delta_{z;drift}^2 + \delta_{z;back}^2$ is approximately 1 nm^2. From the mechanical design, the mechanical stabilities of the stage in the *x* and *z*-directions are similar to each other. The $\delta_{z;drift}^2$ is less than $\Delta x^2 = (0.53 \text{ nm})^2$. The readout noise of the CCD camera (4.5 e^- in the standard deviation) is negligible because the noise was much smaller than the number of electrons in the signal (2000 e^- at the peak), as shown in Fig. 2c. Thus, the *z*-localization error might be deteriorated by the background of emission ($\delta_{z;back}$).

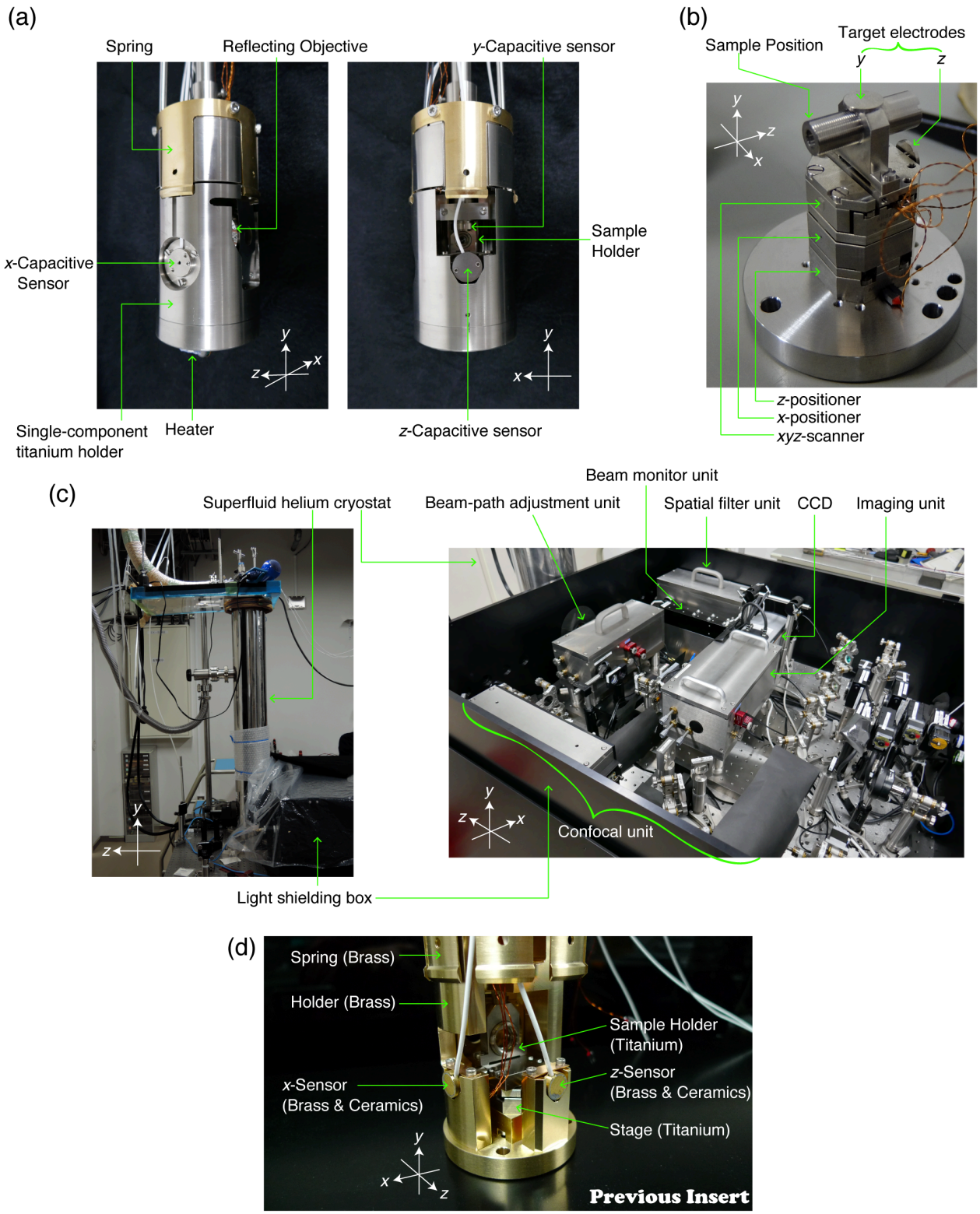

Figure S1. Photographs of the cryo-reflecting microscope. The head of the superfluid helium insert (a), the sample holder and cryogenic piezo-driven stages (b), and the overhead view of the cryo-reflecting microscope (c). To suppress thermal drift, the insert head (a, b) was composed chiefly of titanium. (d) The previously reported cryo-insert holder.[1]

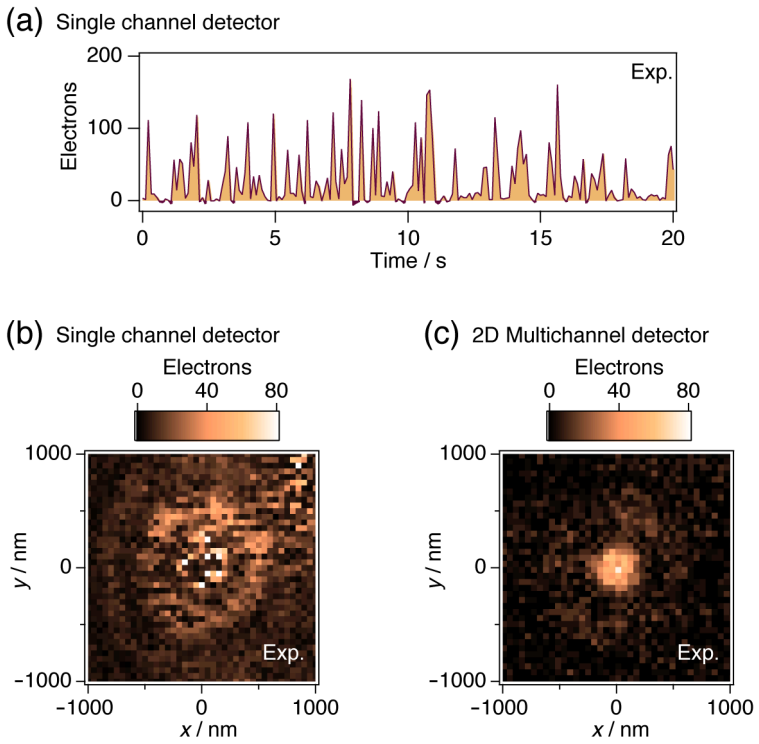

Figure S2. Experimental results for fluorescence blinking of an individual ATTO647N molecule at 1.8 K. (a) The temporal behavior of the fluorescence intensities of an individual ATTO647N molecule was measured with a single-channel detector. The time interval was 0.1 s. (b, c) The fluorescence image of the individual ATTO647N molecule at 1.8 K taken by raster scanning with a single-channel detector (b) and 2D imaging with a multichannel detector (c). The accumulation time was 0.05 s/pixel (b) and 10 s/frame (c). The accumulation time of image c relative to that of image b was adjusted for the two types of measurements to yield similar fluorescence intensities inside the central disk. The excitation wavelength (λ_{ex}) was 637 nm, and the laser intensity on the sample was 0.8 kW/cm^2 in image a, b, and c.

Comment for Fig. S2

In the case of the present cryo-reflecting microscope, fluorescence images of the individual molecule were taken using a 2D multichannel detector to suppress the blinking noise of fluorescence for an individual molecule. The fluorescence of an individual fluorescent molecule often shows a repeated on/off cycle of emission called blinking (Fig. S2a). The blinking noise severely deteriorates the fluorescence image quality when the fluorescence signals at different positions in the image are measured at different points of time. Therefore, an image taken point-by-point with a single-channel detector through raster scanning of the sample is severely influenced by blinking, whereas an image taken with a 2D multichannel detector is free from blinking noise. Figures S2b and S2c compare the fluorescence image of the same ATTO647N molecule taken using raster scanning with a single-channel detector (**b**) and 2D imaging with a multichannel detector (**c**) at 1.8 K. In the raster scanning image, the blinking noise is observed as several black lines along the *x*-axis (the scanning-line direction). The central disk was weakened and the concentric rings were emphasized. By contrast, the signal-to-noise ratio of the multichannel image (Fig. S2c) is apparently better than that of the raster scan image (Fig. S2b). Therefore, in the present work, not only the lateral (*xy*-) localization but also the axial (*z*-) localization of an individual fluorescent molecule was performed using blinking-free images obtained with a 2D multichannel detector.

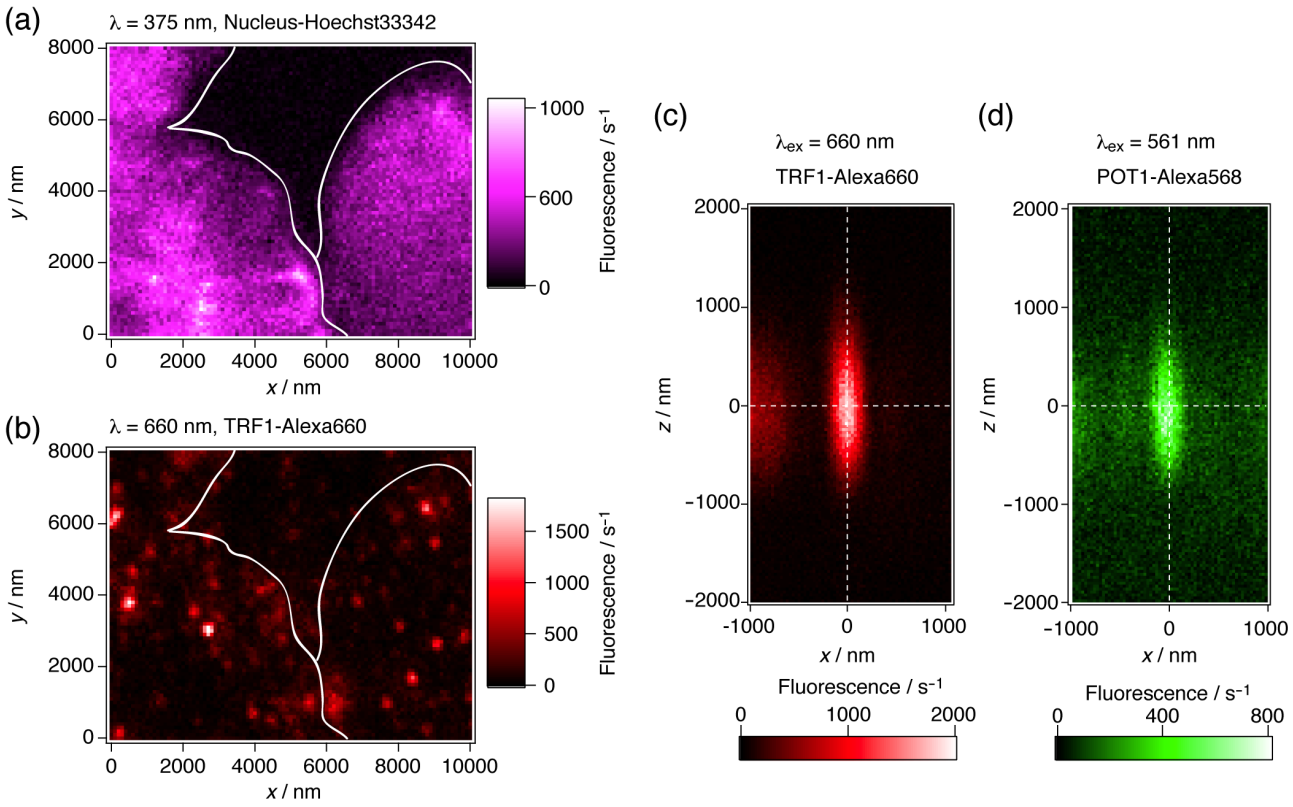

Figure S3. Confocal fluorescence imaging of immunolabeled telomeres in a fixed HeLa cell at 1.9 K. The fluorescence image of a HeLa cell was observed with the confocal raster-scanning mode of the cryo-reflecting microscope (Fig. S4b). The nucleic acid was stained with Hoechst 33342 and imaged with laser light of λ_{ex} = 375 nm (a). Two shelterin proteins, Telomeric Repeat Factor 1 (TRF1) and Protection of Telomere 1 (POT1), were immunolabeled with secondary antibodies of Alexa Fluor 660 and Alexa Fluor 568, respectively. TRF1 (b and c) and POT1 (d) were photo-excited with laser lights of λ_{ex} = 660 nm and 561 nm, respectively. In the image a and b, the edges of the nuclei are shown with white curves. As seen in the images in a and b, individual telomeres were observed as separated fluorescence spots in the nucleus of the cell. One of the telomeres in b was imaged with λ_{ex} = 660 nm (c) and 561 nm (d). The standard deviations of the central disk of the telomere at λ_{ex} = 660 nm were 104 ± 1 nm (s_x), 120 ± 1 nm (s_y), 442 ± 3 nm (s_z). The predicted size of the central disk is s_{xy} = 84 nm and s_z = 360 nm, as estimated from the fluorescence image of an individual quantum dot in a polyvinyl alcohol film at 1.7 K.[1]

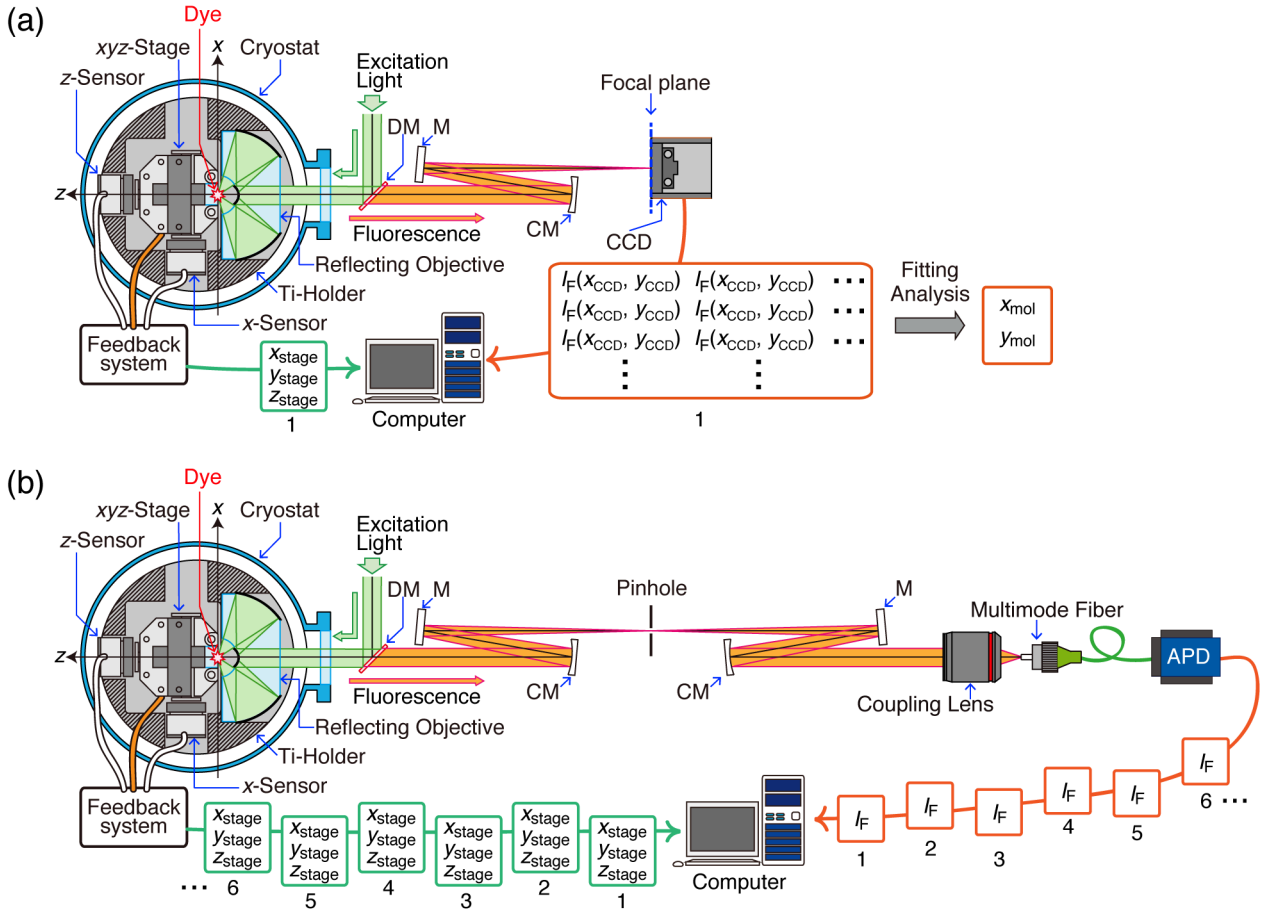

Figure S4. Optical setup of the cryo-reflecting microscope. (a) Configuration for *xy*-localization. (b) Configuration for imaging using confocal raster-scanning imaging (b). Symbols are DM: Dichroic mirror, CM: a silver-coated concave mirror (f_{CM} = 1000 mm), M: a silver-coated flat mirror, CCD: charge coupled device, x_{stage}, y_{stage}, and z_{stage}: the 3D position of the *xyz*-stage measured by capacitive sensors, $I_F(x_{CCD}, y_{CCD})$: the fluorescence intensity on a CCD pixel positioned at x_{CCD} and y_{CCD}, x_{mol} and y_{mol}: the lateral (*xy*-) position of the fluorescent molecule localized using $I_F(x_{CCD}, y_{CCD})$, APD: Avalanche photo-diode detector, I_F: the fluorescence intensity observed with a single channel detector (APD). We operated the cryo-reflecting microscope in three modes, i.e., *xy*-localization (a), confocal raster-scanning imaging (b), and *z*-localization (see Fig. 2a). In the measurement of b, the fluorescence intensity (I_F) of an individual ATTO647N molecule was measured point-by-point with a single-channel photodetector via raster scanning of the sample position (x_{stage}, y_{stage}, z_{stage}). The 3D fluorescence images of the fixed cell (Fig. S3) were observed in confocal imaging mode (b).

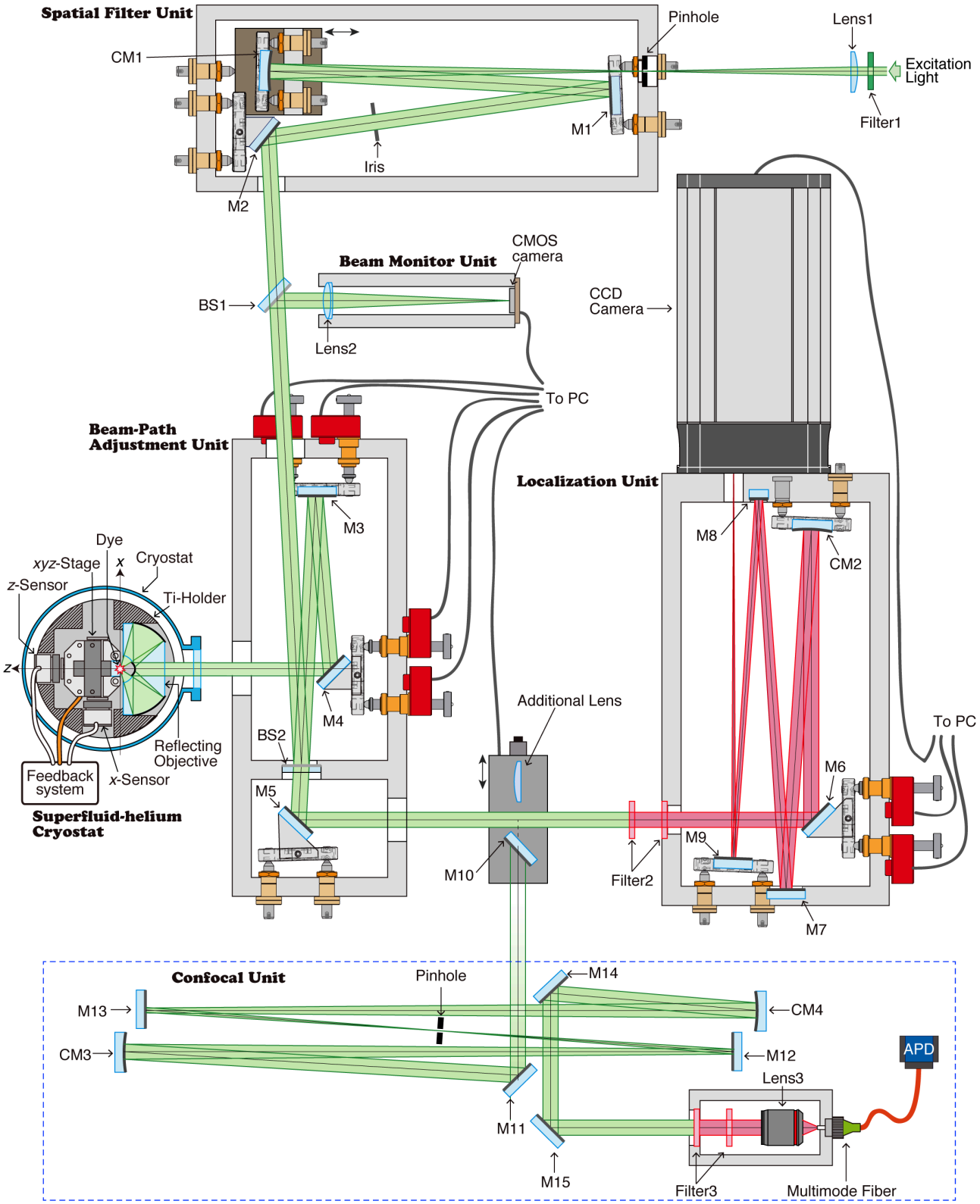

Figure S5. Optical arrangement of the cryo-reflecting microscope. The symbols are M1–15: silver-coated flat mirrors, BS1–2: beam splitters ($T = 0.8$ at $\lambda = 700$ nm), CM1: a silver-coated concave mirror (focal length, $f = 250$ mm), CM2–4: silver-coated concave mirrors (focal length $f = 1000$ mm), APD: Avalanche photo-diode, CMOS: complementary metal oxide semiconductor, CCD: a charge-coupled device.

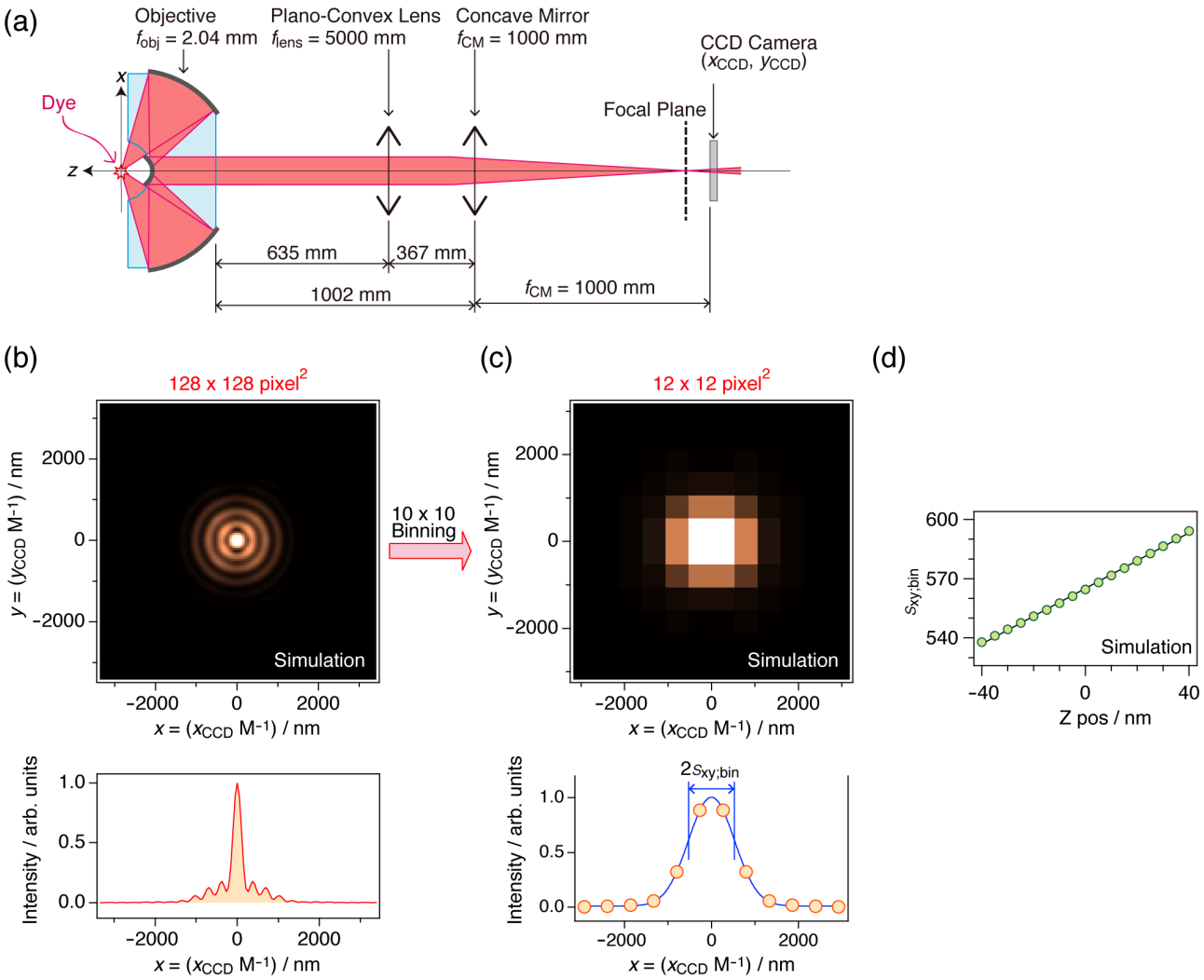

Figure S6. Optical simulation of PSF for fluorescence of an individual molecule in the *z*-localization experiment. (a) Optical layout of the simplified cryo-reflecting microscope for the optical simulation of the *z*-localization mode. (b) Simulated PSF on the CCD camera. The horizontal and vertical axes are the CCD position (x_{CCD}, y_{CCD}) divided by the magnification of the cryo-reflecting microscope (M = 490). The image b was binned into 100 (10 × 10) pixels to obtain the component with low spatial frequency (c). The binned PSF resembles a Gaussian function (blue curve). (d) Standard deviation of the binned PSF ($s_{xy;bin}$) shown as a function of the *z*-position of the fluorescent molecule.

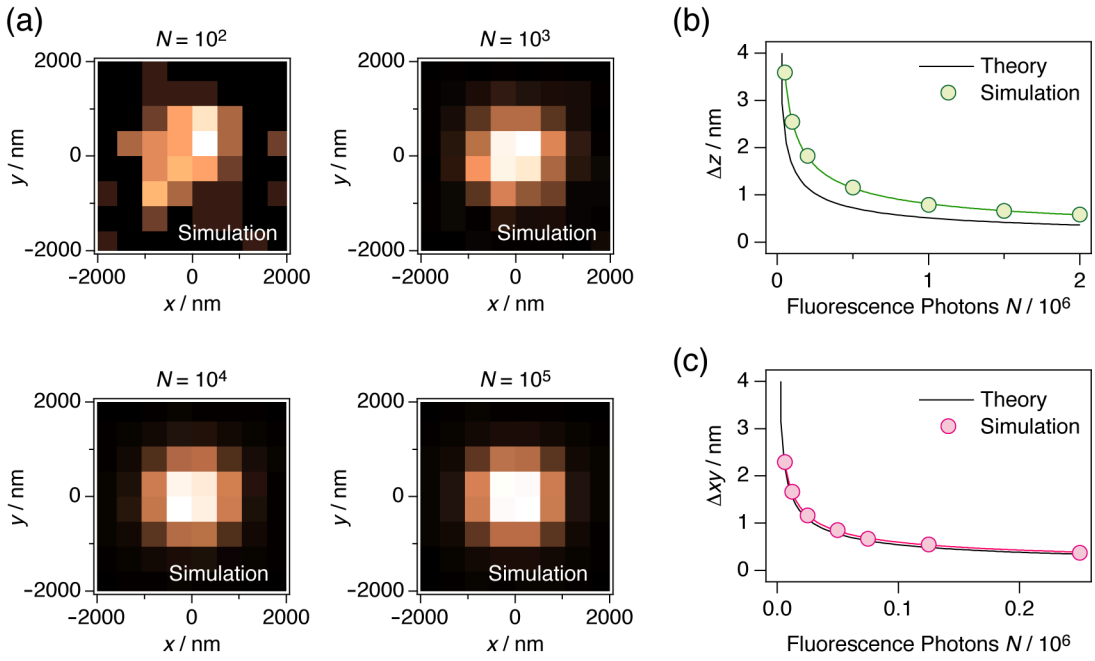

Figure S7. Optical simulation for the standard error of the localization of an individual fluorescent molecule. (a) Poisson-noised images of the binned PSF of an individual fluorescent molecule (Fig. S6c) under the conditions for the fluorescence photons N = 10^2, 10^3, 10^4, and 10^6. Optical simulation for the localization errors of Δz (b) and Δxy (c) as a function of N (colored circles). The theoretical curve is depicted by a black curve.

Table S1. Three-dimensional localization error of cryo-localization microscopy for an individual ATTO647N molecule at 1.8 K.

Axis	Localization Error	t / s	N	s / nm	$A^{exp.}$	$A^{sim.}$	$A^{exp.}$ / $A^{sim.}$
x	0.53 nm	64	0.99×10^6	139	3.8	1.7	2.2
y	0.31 nm	64	0.99×10^6	139	2.2	1.7	1.3
z	0.90 nm	256	3.0×10^6	515	3.0	1.3	2.4

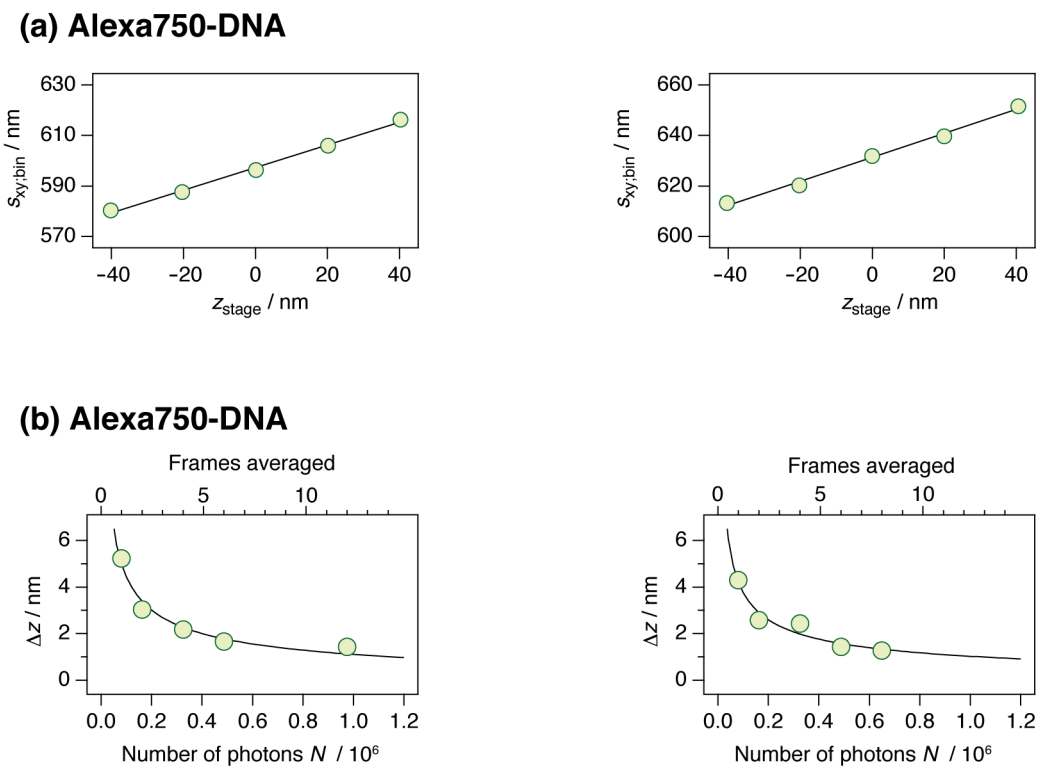

Figure S8. (a) Standard deviation of the binned image ($s_{xy;bin}$) of two Alexa750-DNA molecules at 1.8 K as a function of the stage position (z_{stage}). (b) The *z*-localization error (Δz) of two Alexa 750-DNA molecules at 1.8 K as a function of the number of photons collected (N). We used another reflecting objective (NA = 0.93, f = 2.50 mm); hence the standard deviation $s_{xy;bin}$ is slightly different from Fig. 2d. The excitation wavelength (λ_{ex}) was 730 nm.

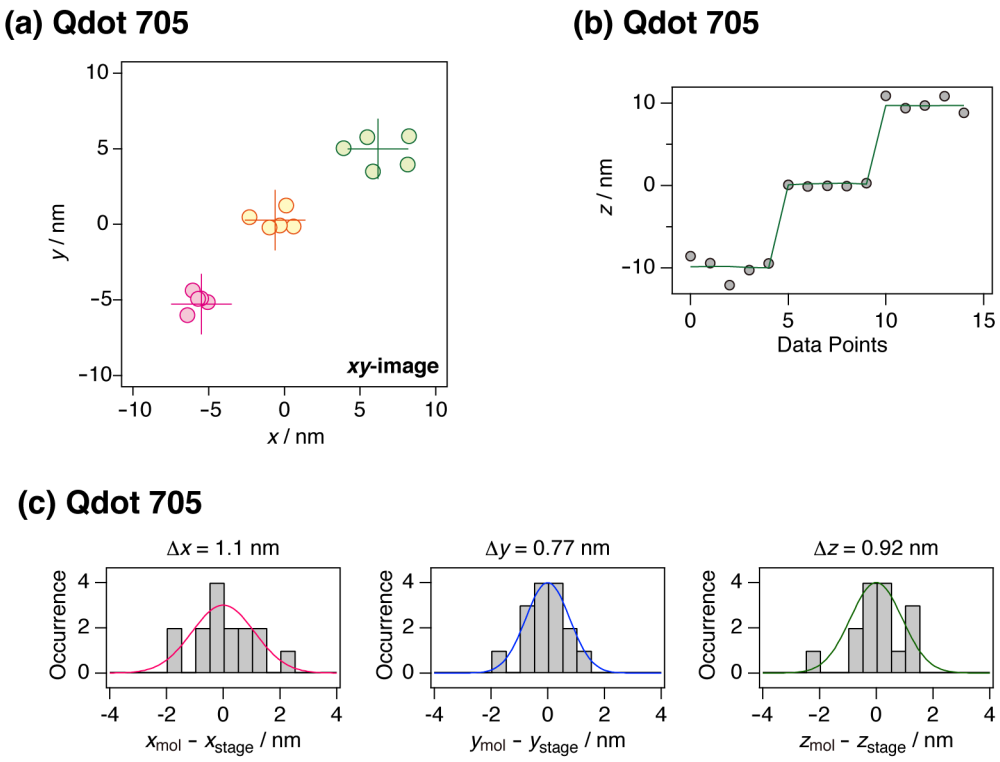

Figure S9. 3D localization of quantum dot (Qdot 705 carboxylic acid, Invtrogen) with λ_{ex} of 637 nm at 1.8 K. (a) The *xy*-image of localized position of the individual quantum dot at three stage positions of (x_{stage}, y_{stage}, z_{stage}) = (–5 nm, –5 nm, 0 nm), (0 nm, 0 nm, 0 nm), and (5 nm, 5 nm, 0 nm). The stage position is indicated by colored crosses. The localized positions of the individual quantum dot are shown in the pink, yellow, and green circles measured at (x_{stage}, y_{stage}, z_{stage}) = (–5 nm, –5 nm, 0 nm), (0 nm, 0 nm, 0 nm), and (5 nm, 5 nm, 0 nm), respectively. (b) The *z*-localized position of another quantum dot at three stage positions (x_{stage}, y_{stage}, z_{stage}) = (0 nm, 0 nm, –5 nm), (0 nm, 0 nm, 0 nm), and (0 nm, 0 nm, 5 nm). The localized positions are indicated by gray circles and the *z*-stage position is shown by green line. The accumulation time *t* per point was 6 s (a) and 256 s (b), and the number of detected photons per point was 1.1×10^5 in (a) and 1.6×10^6 (b). (c) Histograms of the variances between the stage position and localized positions of the individual quantum dots, which are calculated from (a) and (b). The localization errors were evaluated from the variances to 1.1 nm (Δx), 0.77 nm (Δy), and 0.92 nm (Δz).

Supporting References

(1) Inagawa, H.; Toratani, Y.; Motohashi, K.; Nakamura, I.; Matsushita, M.; Fujiyoshi, S. *Sci Rep* **2015**, *5*, 12833.

(2) Thompson, R. E.; Larson, D. R.; Webb, W. W. *Biophys. J.* **2002**, *82*, 2775.

(3) Hirai, Y.; Masutomi, K.; Ishikawa, F. *Genes Cells* **2012**, *17*, 186.

(4) Narita, M.; Nunez, S.; Heard, E.; Narita, M.; Lin, A. W.; Hearn, S. A.; Spector, D. L.; Hannon, G. J.; Lowe, S. W. *Cell* **2003**, *113*, 703.

(5) Bloeß, A.; Durand, Y.; Matsushita, M.; Van der Meer, H.; Brakenhoff, G. J.; Schmidt, J. *J. Microsc.-Oxf.* **2002**, *205*, 76.